SFG Study of the Potential Dependent Adsorption of the P-toluenesulfonate Anion at an Activated Carbon/Propylene Carbonate Interface

Elizabeth K Humphreys[1], Michael T L Casford[1], Phoebe K Allan[2], Clare P Grey[1], Stuart M Clarke[1, 3]*

[1]Department of Chemistry, University of Cambridge, Lensfield Road, Cambridge, CB2 1EW

[2]Gonville and Caius College, Trinity Street, Cambridge, CB2 1TA

[3]BP Institute, University of Cambridge, Madingley Road, Cambridge, CB3 0EZ

ABSTRACT

Sum frequency generation spectroscopy has been used to characterise the potential dependent adsorption of the p-toluenesulfonate anion at the activated carbon/propylene carbonate interface of the commercial carbon YP50F. Spectra recorded from the interface between YP50F and a 1 M tetraethylammonium p-toluenesulfonate in propylene carbonate solution showed no ordered anion adsorption without an applied potential. In contrast, there is clear evidence of increasingly ordered anion adsorption with applied potential. Furthermore there is evidence of hysteresis such that the anion remains adsorbed when the applied potential was decreased back to 0 V. Significant reversal of polarity was required before the anion signal was lost. Changes to the propylene carbonate solvent peaks during the electrochemical cycle were also observed. The data indicate that the positive electrode charges either via a counter-ion adsorption mechanism or via an ion-exchange mechanism.

INTRODUCTION

Electrochemical double layer capacitors (EDLCs) are high power electrical energy storage devices that store charge via the physical mechanism of charge separation. They have extremely long cycle lives and high discharge efficiencies compared to other electrical energy storage technologies, such as batteries or fuel cells.[1–5] They are used in a wide range of applications, from powering small consumer electronics to larger scale applications such as use in hybrid vehicles or cranes.[2–8] Many commercial EDLC electrodes are made from activated carbons. These provide a good balance between the high surface area and electrical conductivity required for good EDLC performance with low cost.[6,9]

While EDLCs have very high power densities, allowing them to be charged and discharged extremely quickly, their energy densities are still notably lower than most batteries. In order to improve EDLCs' energy density, without compromising their power density or their long cycle lives, we need to further our understanding of the electrical double layer (EDL) in which they store their charge.

A wide variety of both modelling and experimental techniques have been applied to address EDLC charging behaviour. Electrochemical measurements have suggested that the details of the charging mechanism and the EDL structure can vary depending on the electrode/electrolyte combination being studied.[10–15] Modelling studies have indicated that at planar interfaces the electrolyte ions adopt a multi-layered structure in which the first layer over-screens the electrode charge.[16–23] Atomic force microscopy, surface force balance and X-ray reflectivity measurements have been used to experimentally examine the EDL structure at planar electrodes and are generally in agreement with the structures predicted by the theoretical studies.[24–29] Modelling of the EDL in porous electrodes has suggested more efficient structures are adopted than at planar

surfaces, allowing greater charge storage capabilities; with appropriate tuning of pore sizes so that they are close to that of the solvated ion, no over-screening occurs increasing capacitance.[23,30–36] Experimental work, carried out using a similar variety of techniques, has also provided evidence for behaviours specific to porous electrodes. Partial electrolyte ion desolvation has been observed using nuclear magnetic resonance spectroscopy (NMR),[37,38] infrared spectroscopy (IR)[39] and by electrochemical quartz crystal microbalance (EQCM) measurements[38,40–42] and electrowetting phenomena have been seen for microporous electrodes using NMR, [43] IR[39] and small angle neutron scattering.[44,45] A number of different charging mechanisms have been proposed for different EDLC systems, which has led to the implication that the details of the charging mechanism depend strongly on the electrode/electrolyte combination being used.[38,40,42,46–49]

Sum frequency generation vibrational spectroscopy is a technique that provides surface specific vibrational spectra. It is based around the non-linear optical phenomenon of sum frequency generation (SFG), which occurs when two incident laser beams overlap at an interface—both spatially and temporally—causing light to be emitted at the sum of the two incident frequencies (as shown in Figure 1).[50,51] SFG spectra are surface specific and can yield information on the conformational order and polar orientation of surface molecules. SFG spectroscopy typically uses a fixed visible laser and a tuneable IR laser. The IR laser probes the vibrational modes of the molecules at the surface and the visible laser shifts the output signal into the visible region. A full mathematical description of SFG can be found elsewhere in the literature. [50,51]

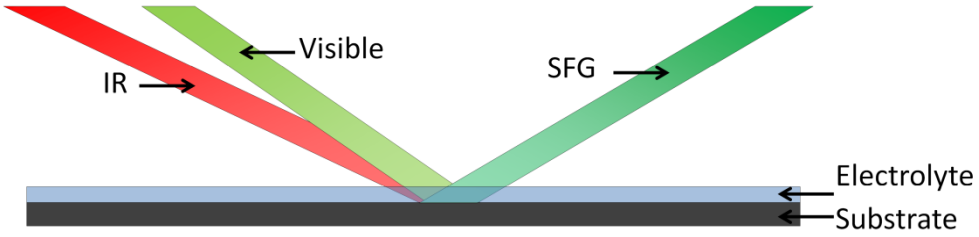

Figure 1: Sum frequency beam generation in a co-propagating geometry. Reflected IR and visible beams are not shown for clarity.

In-situ SFG spectroscopy has been used to studied potential-dependent interfacial behaviour for some time, examining systems ranging from carbon monoxide adsorption on platinum (for catalytic poisoning)[52,53] to metal ions at silica surfaces (for geological applications)[54] to carbonate solvents on $LiCoO_2$ (for lithium ion batteries).[55,56] More recently it has been used to study the EDL in EDLC systems. The majority of these studies have focussed on metal electrodes and ionic liquid electrolytes for simplicity.[57–63] Instead of the multi-layered EDL structure described by other techniques, these works have generally pointed to a structure where the electrode charge is balanced by a highly ordered and strongly bound, Helmholtz like, first layer of ions followed by a 'diffuse layer' with limited structural ordering. A similar lack of long range order has been seen in ex-situ studies of the graphene/ionic liquid interface.[64,65] However, an in-situ investigation of the graphene/1-butyl-3-methylimidazolium dicyanamide ionic liquid by Xu *et al.* observed the more commonly seen multi-layer EDL structure, though it suggested only the first layer contributed to the charge storage mechansim.[66]

While these SFG works have provided some interesting insight into possible potential-dependent EDL structures, we know of no work that has attempted to apply SFG spectroscopy to commercially relevant activated carbon electrode materials. Hence this work will examine the potential-dependent adsorption of the p-toluenesulfonate anion on electrodes made using the

activated carbon YP50F. YP50F and other similar activated carbons have been studied using other techniques—primarily NMR and EQCM—and these have shown a variety of charging mechanisms for both the positive and negative electrodes when in combination with different electrolytes.[49] When using tetraethylammonium tetrafluoroborate in acetonitrile and in propylene carbonate the positive electrode charging mechanism has been seen as a combination of anion adsorption and cation/anion exchange that varies with the applied potential.[40,46,47,67] In contrast, when YP50F electrodes are combined with tetraethylphosphonium tetrafluoroborate in acetonitrile the positive electrode charges by an ion exchange mechanism and with 1-methyl-1-propylpyrrolidinium bis(trifluoromethansulfonyl)imide the positive electrode charging mechanism lies somewhere between pure anion adsorption and ion exchange.[38,68] A similar activated carbon, YP80, has also been observed to have an ion exchange charging mechanism when combined with a number of aqueous electrolytes.[48] While these different studies have demonstrated how the charging mechanism can vary with different electrode/electrolyte combinations, in all cases the positive electrode charging mechanism has involved some degree of anion adsorption (either solely or in combination with loss of cations).

Here an EDLC system made using YP50F electrodes and 1 M tetraethylammonium p-toluenesulfonate in propylene carbonate was studied. The two most common solvents for organic EDLC electrolytes are acetonitrile and propylene carbonate.[5,6] Propylene carbonate was chosen over acetonitrile in this case due to its lower volatility and toxicity. One of the most common salts used to make organic EDLC electrolytes is tetraethylammonium tetrafluoroborate,[5,6] which due to its highly centrosymmetric structure was deemed unlikely to be SFG active. As previous studies have suggested that when using YP50F or other activated carbon electrode materials, the charging mechanism in the positive electrode involves some anion adsorption occurring it was

decided to choose an anion with known SFG activity but to use the tetraethylammonium cation to maintain EDLC performance as much as possible. As such, the p-toluenesulfonate anion was chosen as it both contains known SFG active vibrational modes and its aromatic modes are distinct from any propylene carbonate features occurring in the SFG spectra.[69–71]

EXPERIMENTAL METHODS

Electrolyte solutions were made by dissolving the required mass of tetraethylammonium p-toluenesulfonate (Alfa Aesar, purity 98 %) in propylene carbonate (Sigma Aldrich, anhydrous, purity 99.7 %, water content < 0.002 %). The propylene carbonate (PC) was used as received and the tetraethylammonium p-toluenesulfonate (TEA tosy) was dried *in vacuo* overnight prior to use. The YP50F activated carbon (Kuraray Chemical Company Ltd.) was made into free standing films in the standard way by mixing the carbon powder (95 wt%) with polytetrafluoroethylene (5 wt%) (Sigma Aldrich, 60 wt% dispersion in water).[67,68] Films were dried *in vacuo* at 100 °C overnight prior to use.

SFG spectra were recorded using an Ekspla SFG spectrometer (Nd:YAG laser, 29 ps pulses at 50 Hz) at the Department of Chemistry, University of Cambridge, which generates a visible green beam ($\lambda = 532$ nm) and a mid-IR tunable beam. The two beams are incident on the sample in a co-propagating geometry (with angles of 60 ° and 55 ° to the electrode surface normal for the green and IR beams respectively). YP50F film electrodes were held in a custom designed, symmetric two-electrode EDLC-style cell with a calcium fluoride hemi-cylindrical prism, which is illustrated in the Supplementary Information, Figure S2. Spectra were recorded in SSP and PPP polarisations—where 'S' and 'P' denote beam polarisations perpendicular and parallel to the plane of incidence respectively and describe the beams in the order: SFG, visible, IR. In-situ

electrochemical measurements were carried out using a Metrohm Autolab PGSTAT101 potentiostat. A constant potential was applied to the cell and SFG spectra were recorded once the current had equilibrated. The spectra shown in Figure 2 were recorded without an applied potential. The spectra shown in Figure 3 and Figure 4 were recorded during the first electrochemical cycle of the sample, while the spectra shown in Figure 5, Figure 6 and Figure 7 are part of continuous electrochemical cycle begun with the spectra recorded in Figure 4. Spectra were fitted using the program Baseline2000.

RESULTS

YP50F/PC interface

The SFG spectra recorded in the C-H stretching region for the YP50/PC interface are shown in Figure 2. Although there are a number of SFG spectroscopy studies that use carbonate solvents,[56,72–74] little work has been done investigating PC containing systems and the work that has been done has tended to focus on the carbonyl stretching region.[55] Therefore, the assignment of the peaks in the SFG spectra needs to be made by considering both the SFG spectra of similar molecules and the expected positions of the IR and Raman vibrational bands (IR and Raman spectra shown in the Supplementary Information). For the IR and Raman spectra the peaks around 2880 cm^{-1} and 2940 cm^{-1} have both been given varying assignments as CH_3 and CH_2 stretches.[75–78] In SFG spectra of long purely hydrocarbon tails and of simple alcohol molecules the peak seen around 2880 cm^{-1} is typically assigned to a CH_3 symmetric stretch and the peak seen around 2940 cm^{-1} to the Fermi resonance of the CH_3 symmetric stretch, while the CH_2 stretches occur at slightly different frequencies.[79–81] However, the presence of the five membered ring and the oxygen atoms are likely to shift the peaks relative to simpler hydrocarbon systems.

In diol systems where there are CH_2 groups next to an oxygen atom, as occurs in PC, the CH_2 symmetric stretch occurs around 2865–2870 cm^{-1} and the Fermi resonance of this stretch occurs around 2915–2940 cm^{-1}.[82] Such molecules however still do not include any effects due to the ring structure in PC. Closer molecular analogues would be provided by diethyl carbonate or more particularly by ethylene carbonate (EC). In an SFG study considering both these molecules as the solvent in a battery electrolyte peaks at 2875 cm^{-1} and 2895 cm^{-1} were assigned to CH_3 and CH_2 symmetric stretches respectively and the peak at 2950 cm^{-1} was assigned to the CH_3 asymmetric stretch.[74] A comparison between the YP50/PC and YP50/EC interfaces (shown in the Supplementary Information, Figure S6) shows that while the SFG spectra display peaks in the same positions (around 2880 cm^{-1} and around 2940 cm^{-1}) the relative intensities of the two peaks are different in the two systems in the SSP polarisation. Given the similarity of the spectra of EC and PC we have assigned the peak at 2880 cm^{-1} to the CH_2 symmetric stretch and the peak at 2940 cm^{-1} to the Fermi resonance of the CH_2 stretch, but possibly with some contribution from a CH_3 stretching mode.

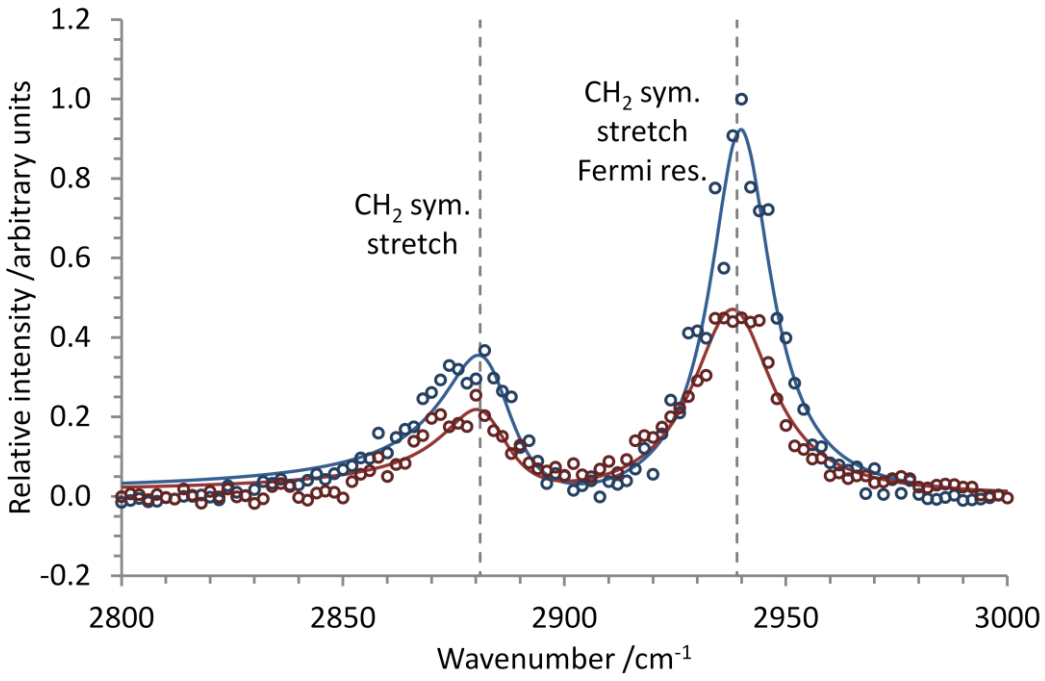

Figure 2: SSP (blue) and PPP (red) SFG spectra of the YP50F/PC interface. Data are shown as hollow points and fits as solid lines.

Since this is the first time YP50F activated carbon has been used as an SFG substrate the spectra shown in Figure 2 can be used to assess whether the carbon film is behaving as a dielectric substrate or not. On dielectric surfaces, CH_3 and CH_2 peak intensity depends on the nature of the vibration. Symmetric stretches are significantly more intense in the SSP polarisation, while the intensity of asymmetric stretches is significantly greater in the PPP polarisation.[82] In contrast to dielectrics, metallic surfaces typically show much stronger signals in the PPP polarisation for all vibrations. The higher intensity of the peaks in the SSP polarisation relative to the PPP polarisation confirms that the YP50F carbon film is not behaving as a metallic substrate. This is to be expected as it lacks the ordered metallic structure required for the plasmonic resonances that give rise to the high PPP polarisation intensity on metallic substrates. However, the reduction in peak intensity in the PPP spectrum compared to the SSP spectrum is

somewhat smaller than might be expected if the YP50F carbon film were behaving in a purely dielectric manner.[82,83] This presumably stems from two factors. Firstly, the conducting nature of the carbon powder prevents the film from being a truly dielectric surface. Secondly, the polarization behaviour at dielectric interfaces is not expected to match the behaviour at electrochemical interfaces[82] and here the YP50F carbon film is acting as an electrochemical interface.

Further to considering the dielectric/metallic character of YP50F under SFG spectroscopy, it must also be determined whether the SFG signal arises primarily from the internal or external surface of the carbon. As an activated carbon YP50F has a very large surface area and high porosity. As such the internal surface area makes up a high proportion of the total surface area. However, as a carbon black it also strongly absorbs visible light. This will not only limit the penetration depth of the incident green laser beam, but will significantly limit the depth from which SFG signals can detected. Hence it might be expected that only surface area in the top few tens to hundreds of nanometres are contributing to the SFG signal. Within such a depth range the external surface area of the film plays a more substantial role than if the full depth was being probed. For those pores close enough to the surface to be accessible to SFG spectroscopy the symmetry conditions for SFG activity must be considered. Any pores large enough for ions to adsorb on both the top and bottom surfaces are likely to act as macroscopically centrosymmetric and so not give rise to any SFG signals. The centrosymmetry of smaller pores is likely to be highly dependent on the orientation of the occupying electrolyte species. However, between the limited penetration depth of the SFG signals and the likely lack of SFG activity in some if not all of the pore spaces, we conclude that the signal seen in the recorded SFG spectra are likely to be primarily from the external surface of the film.

Initial YP50F/1 M TEA tosy in PC electrolyte solution interface

Figure 3 shows the C-H stretching region SFG spectra recorded for the YP50F/1 M TEA tosy in PC electrolyte solution interface with and without an applied potential of 2 V (spectra recorded on the positive electrode, peak assignments given in Table 1). Without an applied potential the YP50F/electrolyte solution spectrum is very similar to the YP50F/pure PC spectrum, showing peaks at 2940 cm^{-1} and 2880 cm^{-1} but with no evidence of ordered tosy anion adsorption. With the application of the potential, the PC C-H stretches at 2940 and 2880 cm^{-1} both show a reduction in intensity and a shift to lower wavenumber. However, the main difference in the spectra on the application of a voltage is the appearance of a peak around 3060 cm^{-1}, which has been assigned to a combination of the tosy anion aromatic methyne (CH) stretching modes.[69,71,84,85] The appearance of this peak indicates that ordered adsorption of the anion is occurring on the application of a positive potential. The causes of the changes to the PC peaks are more ambiguous. The intensity reduction may be due to a change in molecular ordering or orientation, but may equally well suggest a loss of solvent from the surface. This in turn may suggest that the tosy anion is directly adsorbed onto the carbon surface without a solvation layer, displacing some of the solvent molecules. As discussed above, the SFG signal is likely to come primarily from external surface area so the tosy anion adsorption indicated by this spectrum is also likely to be occurring at the external surface of the carbon.

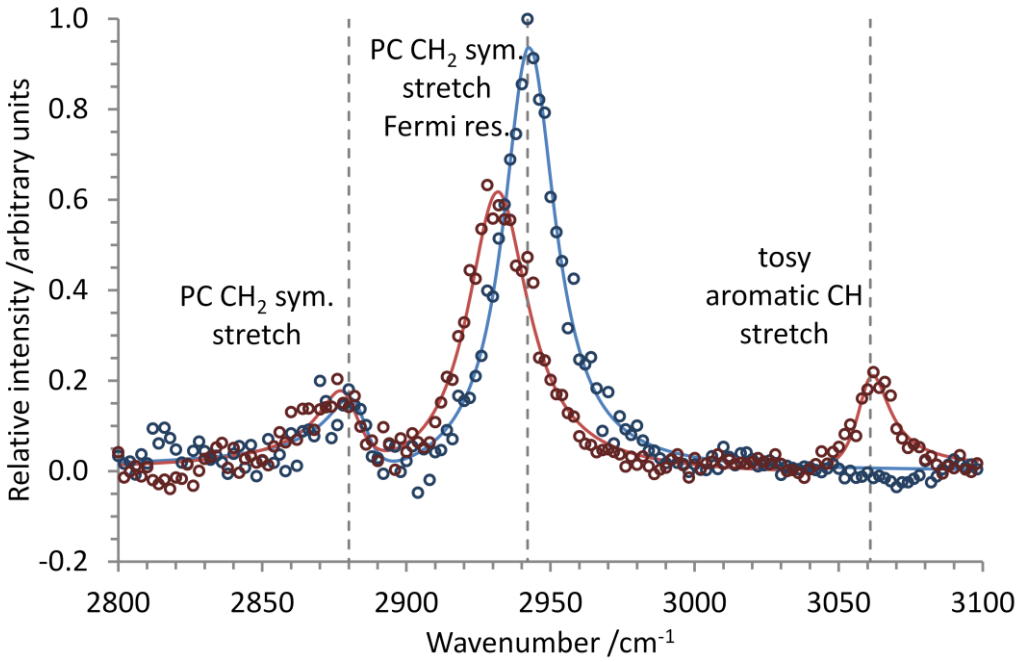

Figure 3: Comparison of the the YP50F/1 M TEA tosy in PC electrolyte solution interface SFG spectra recorded without an applied potential (blue) and with a 2 V applied potential (red). Spectra were recorded at the positive electrode in the SSP polarisation. Data are shown as hollow points and fits as solid lines.

Table 1: Peak details from the positive electrode YP50F/1 M TEA tosy in PC interface SFG spectra with and without an applied potential.

Applied Potential	Peak centre /cm^{-1}	Relative peak area	FWHM /cm^{-1}	Peak Assignment
0 V	2942	10.28	21.96	PC CH_2 stretch (symmetric)
	2884	1.00	15.87	PC CH_2 stretch (sym. Fermi res.)[a]
2 V	3061	2.05	13.81	Tosy aromatic CH stretch

	2931	6.73	25.83	PC CH_2 stretch (symmetric)
	2880	1.00	17.28	PC CH_2 stretch (sym. Fermi res.)[a]

[a]This peak may also contain some contribution from a CH_3 stretching mode

In order to verify that the signal seen in the SFG spectra was coming from the YP50F/electrolyte solution interface and not the prism/electrolyte solution interface, a comparison of the two systems was recorded, the results of which are given in the Supplementary Information, Figure S8. The spectra recorded at the prism/electrolyte solution interface showed a considerably reduced intensity compared to the YP50F/electrolyte solution interface. The change is significant enough in magnitude that the signal seen in the YP50F/electrolyte spectra can be confidently assigned to the interface of interest.

Potential dependence of the YP50F/1 M TEA tosy in PC electrolyte solution interface

Further to the simple comparison between spectra recorded at the positive electrode with and without an applied potential, spectra were recorded at multiple applied voltages between 0 and 2 V during both the charge and discharge halves of a first electrochemical cycle. Figure 4 shows the spectra recorded during charging (the peak details are given in the Supplementary Information). The initial 0 V spectrum shows the expected PC peaks at 2880 cm^{-1} and 2940 cm^{-1} and no 3060 cm^{-1} tosy anion peak. The anion peak appears when the first potential of 0.5 V is applied to the sample and it continues to grow as the applied potential is increased. Interestingly however, the intensity change is not a linear function with increasing applied potential. Since peak intensity correlates with both species number density and with how well ordered a species is this increasing intensity could relate to an increase in either the quantity of tosy anions at the YP50F surface or the ordering of the anions. Given that the peak intensity in SSP polarisared

spectra is generally less sensitive to orientational changes than in PPP polarised spectra, the scale of the change (just under a 3 fold increase between the 0.5 V spectrum and the 2.0 V spectrum) suggests that it is not solely based on increased ordering, but that there is an increase in the number of tosy anions present at the YP50F interface. In addition to the intensity increase, the peak centre undergoes a slight shift to higher wavenumber with increasing voltage. This may indicate a subtle change in the adsorption as the applied potential is increased—either an increase in the strength of the adsorption forces or a change in orientation of the adsorption to accommodate an increasing number of ions at the surface.

Further to the changes to the 3060 cm^{-1} peak, the PC peaks at 2940 cm^{-1} and 2880 cm^{-1} show some variation during the charging process. Both the PC related peaks shift to lower wavenumber during charging, though the shift in the 2940 cm^{-1} peak is slightly larger. The intensity behaviour of the PC peaks is more complex. While both peaks exhibit a notable initial drop in intensity when the first potential (0.5 V) is applied, the 2940 cm^{-1} peak intensity then proceeds to recover back to nearly its original value while the 2880 cm^{-1} peak intensity remains roughly constant at its 0.5 V value. The final intensity values at 2.0 V are in general agreement with those seen in the simple 0.0 V/2.0 V comparison. The intensity changes continue to indicate that the potential does lead to changes in the adsorption behaviour of the PC. However, without more detailed information, no concrete conclusion can be drawn as to what those changes might be and whether they involve a change in the number density of PC at the YP50F surface.

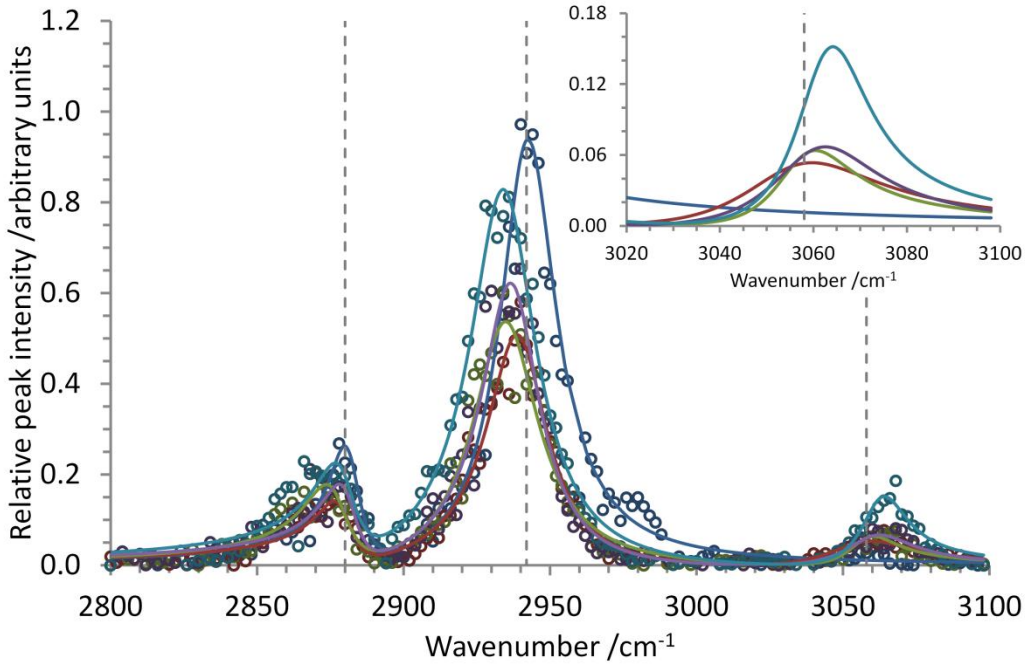

Figure 4: SFG spectra of the YP50F/1 M TEA tosy in PC electrolyte solution positive electrode interface recorded during charging at 0 V (blue), 0.5 V (red), 1.0 V (green), 1.5 V (purple) and 2.0 V (aqua). The inset shows a magnification of the 3020–3100 cm^{-1} region.

The spectra recorded during the first discharge are shown in Figure 5, from which it is clear that the changes seen during discharge are not simply the reverse of those seen during the first charge (peak details given in the Supplementary Information). While the 3060 cm^{-1} tosy anion peak reduces in intensity during discharge, there is still a very definite peak present when the voltage is returned to 0 V. Furthermore, the intensity change follows a much more linear relationship with the applied potential than was observed during charging. Also in contrast to the charging behaviour, the peak centre remains essentially constant, rather than returning back to its initial value. The continued presence of the tosy peak at full discharge indicates that some of the anions remain at the surface even in the fully discharged state.

The intensity of 2940 cm^{-1} peak shows a gradual decrease in intensity, reversing the behaviour seen between 0.5 V and 2.0 V on charge. When the system returns to 0 V, the 2940 cm^{-1} peak intensity is similar to its value at 0.5 V during charge. However, while the 2940 cm^{-1} peak intensity behaviour on discharge seems to relate to that on charge (from 0.5 V onwards), the intensity of the 2880 cm^{-1} peak remains roughly constant throughout discharging. Additionally, in contrast to the charging behaviour, the positions of both peaks remain essentially unchanged.

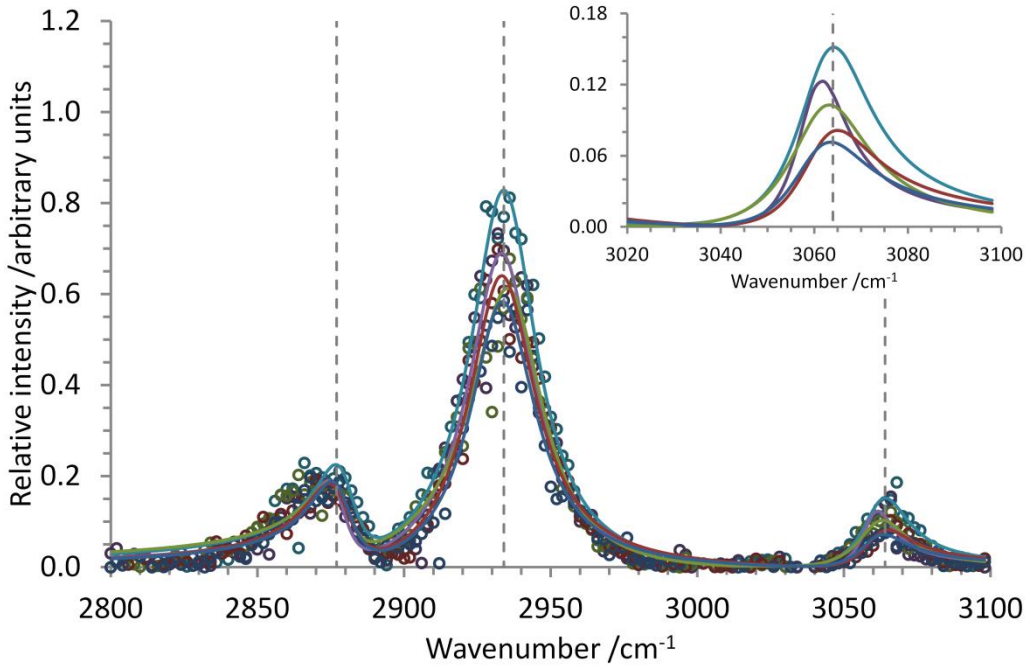

Figure 5: SFG spectra of the YP50F/1 M TEA tosy in PC electrolyte solution positive electrode interface recorded during discharging at 2.0 V (aqua), 1.5 V (purple) , 1.0 V (green), 0.5 V (red) and 0 V (blue). The inset shows a magnification of the 3020–3100 cm^{-1} region.

The effect of reversing the electrode polarity, charging the initially positive electrode to negative potentials, was also investigated. The spectra recorded during the reverse polarity charge are shown in Figure 6 (peak details for these spectra and those shown in Figure 7 are given in the Supplementary Information). The tosy anion peak at 3060 cm^{-1} remains present at

0.5 V (albeit at lower intensity than previously seen) and disappears in the 1.0 V spectrum. This indicates that by 1.0 V on the reverse polarity charge the ordered tosy anion adsorption can no longer be sustained, suggesting that it is driven off the surface as the negative charge on the carbon increases.

The intensity of the 2940 cm^{-1} PC peak shows a nearly 3 fold increase during the reverse polarity charge that is relatively linear with applied voltage. The peak intensity at 2.0 V in the reverse charge is notably higher than at any point seen in the first charge/discharge cycle. The peak also shifts slightly to higher wavenumber, reversing the shift seen during the initial charge. The 2880 cm^{-1} peak also shows a reasonably steady increase in intensity with applied potential, however its increase is much smaller than that of the 2940 cm^{-1} peak. In contrast, the shift in peak position is much more comparable between the two peaks. Additionally, at 2.0 V a new peak appears around 2910 cm^{-1} and the peak shape of the 2940 cm^{-1} peak is asymmetrically broadened, suggesting the presence of a second additional peak around 2925 cm^{-1}.

There are a number of possible explanations for the PC peak behaviour and the appearance of the two new peaks. One is that the changes relate purely to changes in PC adsorption behaviour. These may stem from the removal of the tosy anion giving more space for PC adsorption or from the presence of TEA cations that keep a full solvation shell on adsorption, leading indirectly to an increase of PC at the carbon surface. A second possible explanation is that direct TEA cation adsorption is occurring at the now negative electrode in such a manner as to break the cation's symmetry and allow some of its vibrational modes to become SFG active. As the C-H stretching modes of tetraalkylammonium cations occur at similar frequencies to the PC modes,[86–88] if these modes were to become active they might interfere with the PC modes, changing their appearance. However, where spectra from TEA cations have been recorded only a single, low

intensity peak around 2950 cm^{-1} has been seen,[89] rather than the multiple new peaks recorded here suggesting this explanation is less likely than changes to the PC adsorption. A further possible explanation for the change would be the presence of $\chi^{(3)}$ effects introduced by the strong electric field. These can lead to bulk solution contributions becoming visible in the SFG spectra. However, the asymmetry of the growth of the PC peaks at 2940 cm^{-1} and 2880 cm^{-1}, the lack of any tosy anion contribution from 1.0 V onwards and the lack of any bulk contributions seen during the initial charge/discharge cycle makes this explanation unlikely.

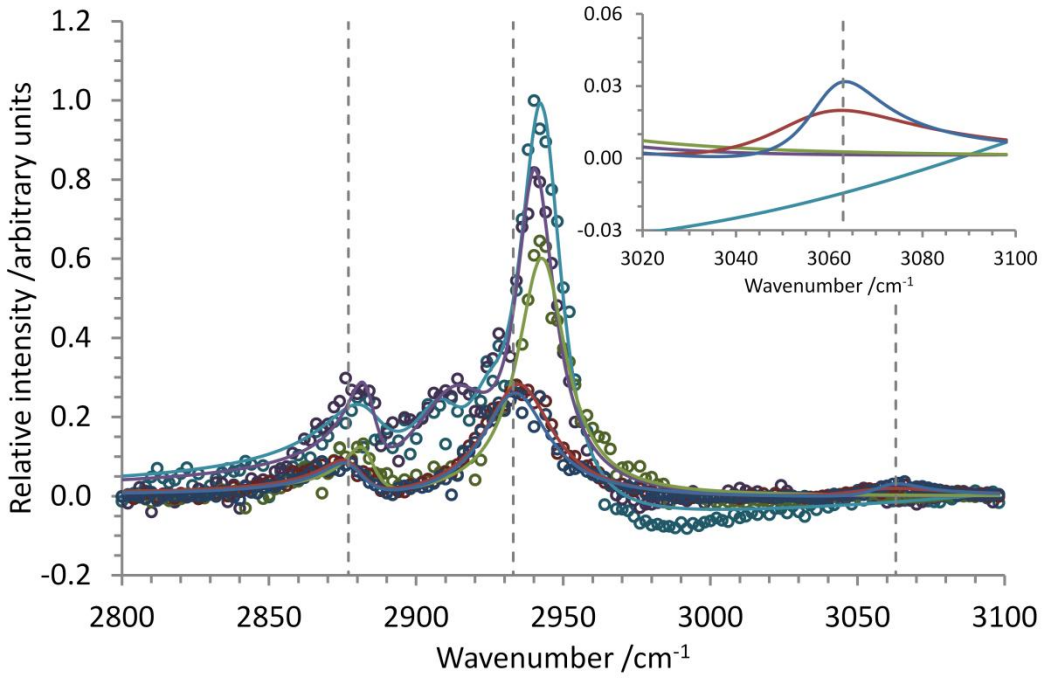

Figure 6: SFG spectra of the YP50F/1 M TEA tosy in PC electrolyte solution (now) negative electrode interface recorded during reverse polarity charging at 0 V (blue), 0.5 V (red), 1.0 V (green), 1.5 V (purple) and 2.0 V (aqua).

Figure 7 shows the spectra recorded during the reverse polarity discharge. The tosy anion 3060 cm^{-1} peak remains absent from these spectra, which is expected as it only appeared on the application of a positive potential to the interface. However, the new peak at 2910 cm^{-1} and the

asymmetry of the 2940 cm^{-1} peak that appeared during the reverse polarity charge remain present throughout the discharge half of the cycle and are still visible at complete discharge to 0.0 V. The 2940 cm^{-1} peak decreases in intensity, in a reasonably linear fashion with the applied potential, but at a slower rate than the increase in intensity seen during the reverse polarity charge. The final intensity value of the 2940 cm^{-1} peak is still larger than the initial intensity value before cycling was begun. In contrast the peak position undergoes a very small shift to lower frequencies to return to essentially the original recorded wavenumber. The 2880 cm^{-1} peak intensity continues to increase during the reverse polarity discharge, however its position remains essentially constant. Again, an exact assignment of the causes of the changes to the PC peaks cannot be concluded from the information recorded in the current spectra.

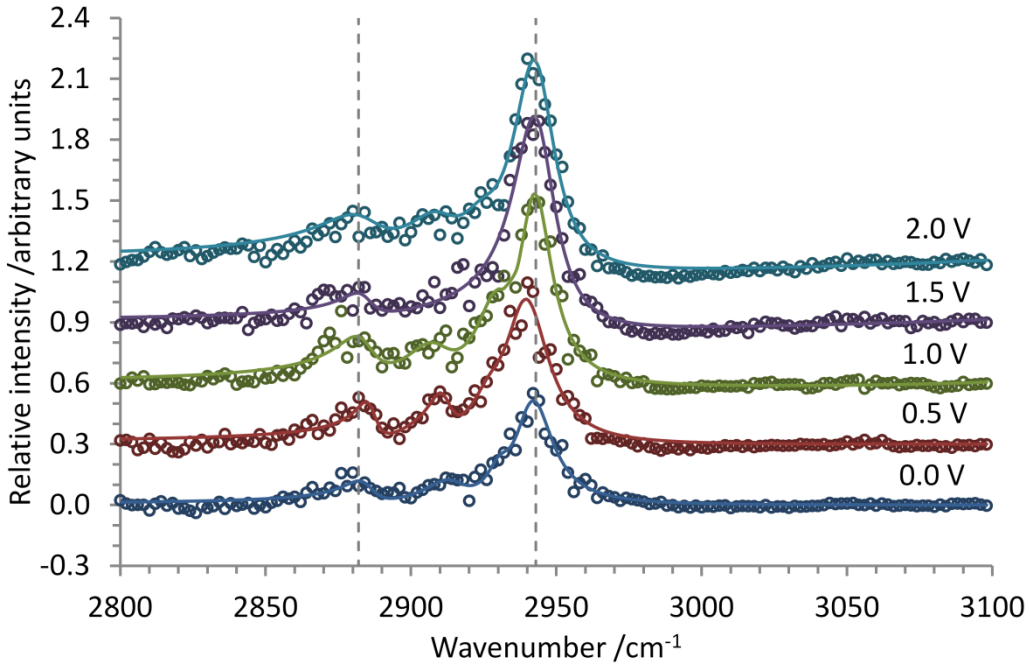

Figure 7: SFG spectra of the YP50F/1 M TEA tosy in PC electrolyte solution (now) negative electrode interface recorded during reverse polarity discharge at 2.0 V (aqua), 1.5 V (purple), 1.0 V (green), 0.5 V (red) and 0 V (blue).

DISCUSSION

The changes to the spectra recorded during the first and reverse polarity charge/discharge cycles can begin to provide insights into the charging behaviour of the YP50F electrode, 1 M TEA tosy in PC electrolyte solution system. The physical charge storage occurring in EDLCs can be achieved by a range of different mechanisms, using different counter-ion/co-ion ratios to balance the electrode charge.[49] The two extremes of this range are pure counter-ion adsorption and pure co-ion expulsion. In pure counter-ion adsorption the number of co-ions remains unchanged and the electrode change is balanced by the adsorption of additional counter-ions at the electrode surface, while in pure co-ion expulsion the number of counter-ions remains constant but co-ions are expelled from the surface (with the changes in ion concentration being accompanied by changes in amount of solvent present at the surface to obey volumetric constraints). Pure ion exchange would lie exactly in the middle of these, combining equal numbers of additional adsorbed counter-ion and expelled co-ions.

The ordered tosy anion adsorption seen during the initial charge cycle shows that the positive electrode cannot be operating by a pure co-ion expulsion mechanism. Furthermore, it suggests a mechanism between counter-ion adsorption and ion-exchange. Moreover, the non-linear behaviour of the peak intensity suggests that the charging mechanism may vary with applied potential. The rapid intensity increase between 1.5 V and 2.0 V during the initial charge compared to the much more gradual increase from 0.0 V to 1.5 V may suggest that, at least for the first cycle, the degree of anion adsorption is greater at higher potentials. This would imply that the charge storage mechanism moves more towards a pure counter-ion adsorption behaviour as the applied potential is increased. Such a change in charge storage mechanism with applied

potential has been seen before for carbon electrodes combined with organic electrolyte solutions using EQCM measurements.[40,49,90]

The difference in the tosy anion 3060 cm^{-1} peak behaviour seen during charging and discharging in the initial cycle may also suggest that different mechanisms dominate the different halves of the cycle (at least for the first cycle). It also indicates that some of the changes occurring during the first charge may be irreversible, either with some form of irreversible adsorption of the anions at the YP50F surface or with electrowetting providing access to a greater proportion of the electrode's surface area. Such electrowetting has been observed for a similar system—activated carbon electrodes combined with tetraethylammonium tetrafluoroborate in acetonitrile electrolyte solution—using both NMR and small angle neutron scattering, particularly during first cycle charging.[43,45] An irreversible change during the first charge cycle may also explain the different mechanisms acting during charging and discharging.

Furthermore, the persistence of the tosy anion peak to negative voltages, along with some of the changes observed for the PC peaks, suggest that there is a degree of hysteresis within the charging (at least when a full cycle involving a reversal of the electrode polarity is considered). Such a hysteresis has been seen previously with SFG spectroscopy for ionic liquids on platinum electrodes.[59] As with the initial irreversibility of the tosy adsorption, this may be specific to the first cycle due to a phenomenon such as electrowetting.

CONCLUSIONS

We have measured the potential dependent absorption of the tosy anion at the YP50F activated carbon/1 M TEA tosy in PC electrolyte solution interface using SFG spectroscopy. SFG spectra were recorded for the YP50F/electrolyte solution interface at multiple points during a first

charge/discharge cycle to positive potentials followed by a reverse polarity charge/discharge cycle to negative potentials. The tosy anion was found not to exhibit ordered adsorption at the YP50F surface before the application of a potential but ordered, potential dependent, absorption was seen on the application of a positive potential. The results indicated that the positive electrode in EDLCs formed of YP50F electrodes and 1 M TEA tosy in PC electrolyte solution store charge via a mechanism that involves some degree of counter-ion adsorption (somewhere between counter-ion adsorption and ion exchange) and that the charge storage mechanism may be potential dependent. The discharge half of the initial cycle and the reverse polarity charge/discharge cycle indicated that some of the changes occurring at the YP50F surface during the initial positive charge were irreversible and that there was a degree of hysteresis in the full electrochemical cycle from positive to negative voltages.

AUTHOR INFORMATION

Corresponding Author

*S. M Clarke – stuart@bpi.cam.ac.uk

Author Contributions

The manuscript was written through contributions of all authors. All authors have given approval to the final version of the manuscript.

ASSOCIATED CONTENT

Supporting Information. Structures of electrolyte solution component molecules; details of electrochemical SFG cell; IR and Raman spectra of electrolyte solution and its components; SFG spectra of YP50F/PC interface in the 1300−1900 cm^{-1} region; peak details for YP50F/PC interface spectra; comparison of YP50F/1 M TEA tosy in PC solution interface and prism/1 M TEA tosy in PC solution interface spectra; peak details for YP50F/1 M TEA tosy in PC solution during initial charge and discharge and during reverse polarity charge and discharge.

The following files are available free of charge: Supplementary Information (.pdf)

ACKNOWLEDGMENT

We thank Kuraray Chemical Company Ltd. for providing the YP50F activated carbon.

E.K.H. acknowledges the European Research Council ERC Grant ERC-2009-AdG-247411 for funding.

ABBREVIATIONS

EDLC, electrochemical double layer capacitor; EDL, electrical double layer; NMR, nuclear magnetic resonance; IR, infrared spectroscopy, EQCM, electrochemical quartz-crystal microbalance; SFG, sum frequency generation; PC, propylene carbonate; TEA tosy, tetraethylammonium p-toluenesulfonate; CH_3, methyl; CH_2, methylene; CH, methyne

REFERENCES

(1) Conway, B. E. *Electrochemical Supercapacitors: Scientific Fundementals and Technological Applications*; Kluwer Academic/Plenum, 1999.

(2) Kotz, R.; Carlen, M. Principles and Applications of Electrochemical Capacitors.

Electrochim. Acta **2000**, *45* (15–16), 2483–2498.

(3) Miller, J. R.; Burke, A. F. Electrochemical Capacitors: Challenges and Opportunities for Real-World Applications. *Electrochem. Soc. Interface* **2008**, *17* (1), 53–57.

(4) Miller, J. R.; Simon, P. Electrochemical Capacitors for Energy Management. *Science* **2008**, *321* (5889), 651–652.

(5) Simon, P.; Gogotsi, Y. Capacitive Energy Storage in Nanostructured Carbon–Electrolyte Systems. *Acc. Chem. Res.* **2013**, *46* (5), 1094–1103.

(6) Simon, P.; Gogotsi, Y. Materials for Electrochemical Capacitors. *Nat. Mater.* **2008**, *7* (11), 845–854.

(7) Chen, H.; Cong, T. N.; Yang, W.; Tan, C.; Li, Y.; Ding, Y. Progress in Electrical Energy Storage System: A Critical Review. *Prog. Nat. Sci.* **2009**, *19* (3), 291–312.

(8) Luo, X.; Wang, J.; Dooner, M.; Clarke, J. Overview of Current Development in Electrical Energy Storage Technologies and the Application Potential in Power System Operation. *Appl. Energy* **2015**, *137*, 511–536.

(9) Zhang, L. L.; Zhou, R.; Zhao, X. S. Carbon-Based Materials as Supercapacitor Electrodes. *J. Mater. Chem.* **2009**, *38* (29), 2520–2531.

(10) Vix-Guterl, C.; Frackowiak, E.; Jurewicz, K.; Friebe, M.; Parmentier, J.; Béguin, F. Electrochemical Energy Storage in Ordered Porous Carbon Materials. *Carbon* **2005**, *43* (6), 1293–1302.

(11) Chmiola, J.; Yushin, G.; Gogotsi, Y.; Portet, C.; Simon, P.; Taberna, P.-L. Anomalous

Increase in Carbon Capacitance at Pore Sizes Less Than 1 Nanometer. *Science* **2006**, *313* (5794), 1760–1763.

(12) Raymundo-Pinero, E.; Kierzek, K.; Machnikowski, J.; Beguin, F. Relationship Between the Nanoporous Texture of Activated Carbons and Their Capacitance Properties in Different Electrolytes. *Carbon* **2006**, *44* (12), 2498–2507.

(13) Lin, R.; Taberna, P. L.; Chmiola, J.; Guay, D.; Gogotsi, Y.; Simon, P. Microelectrode Study of Pore Size, Ion Size, and Solvent Effects on the Charge/Discharge Behavior of Microporous Carbons for Electrical Double-Layer Capacitors. *J. Electrochem. Soc.* **2009**, *156* (1), A7–A12.

(14) Segalini, J.; Daffos, B.; Taberna, P. L.; Gogotsi, Y.; Simon, P. Qualitative Electrochemical Impedance Spectroscopy Study of Ion Transport into Sub-Nanometer Carbon Pores in Electrochemical Double Layer Capacitor Electrodes. *Electrochim. Acta* **2010**, *55* (25), 7489–7494.

(15) Segalini, J.; Iwama, E.; Taberna, P.-L.; Gogotsi, Y.; Simon, P. Steric Effects in Adsorption of Ions from Mixed Electrolytes into Microporous Carbon. *Electrochem. Commun.* **2012**, *15* (1), 63–65.

(16) Lanning, O. J.; Madden, P. A. Screening at a Charged Surface by a Molten Salt. *J. Phys. Chem. B* **2004**, *108* (30), 11069–11072.

(17) Fedorov, M. V.; Kornyshev, A. A. Ionic Liquid near a Charged Wall: Structure and Capacitance of Electrical Double Layer. *J. Phys. Chem. B* **2008**, *112* (38), 11868–11872.

(18) Feng, G.; Huang, J.; Sumpter, B. G.; Meunier, V.; Qiao, R. Structure and Dynamics of

Electrical Double Layers in Organic Electrolytes. *Phys. Chem. Chem. Phys.* **2010**, *12* (20), 5468–5479.

(19) Vatamanu, J.; Borodin, O.; Smith, G. D. Molecular Insights into the Potential and Temperature Dependences of the Differential Capacitance of a Room-Temperature Ionic Liquid at Graphite Electrodes. *J. Am. Chem. Soc.* **2010**, *132* (42), 14825–14833.

(20) Feng, G.; Huang, J.; Sumpter, B. G.; Meunier, V.; Qiao, R. A "Counter-Charge Layer in Generalized Solvents" Framework for Electrical Double Layers in Neat and Hybrid Ionic Liquid Electrolytes. *Phys. Chem. Chem. Phys.* **2011**, *13* (32), 14723–14734.

(21) Merlet, C.; Salanne, M.; Rotenberg, B.; Madden, P. A. Influence of Solvation on the Structural and Capacitive Properties of Electrical Double Layer Capacitors. *Electrochim. Acta* **2013**, *101*, 262–271.

(22) Paek, E.; Pak, A. J.; Hwang, G. S. A Computational Study of the Interfacial Structure and Capacitance of Graphene in [BMIM][PF6] Ionic Liquid. *J. Electrochem. Soc.* **2013**, *160* (1), A1–A10.

(23) Fedorov, M. V.; Kornyshev, A. A. Ionic Liquids at Electrified Interfaces. *Chem. Rev.* **2013**, *114* (5), 2978–3036.

(24) Atkin, R.; Borisenko, N.; Drüschler, M.; El-Abedin, S. Z.; Endres, F.; Hayes, R.; Huber, B.; Roling, B. An In Situ STM/AFM and Impedance Spectroscopy Study of the Extremely Pure 1-Butyl-1-Methylpyrrolidinium Tris(pentafluoroethyl)trifluorophosphate/Au(111) Interface: Potential Dependent Solvation Layers and the Herringbone Reconstruction. *Phys. Chem. Chem. Phys.* **2011**, *13* (15), 6849–6857.

(25) Hayes, R.; Borisenko, N.; Tam, M. K.; Howlett, P. C.; Endres, F.; Atkin, R. Double Layer Structure of Ionic Liquids at the Au(111) Electrode Interface: An Atomic Force Microscopy Investigation. *J. Phys. Chem. C* **2011**, *115* (14), 6855–6863.

(26) Carstens, T.; Hayes, R.; Abedin, S. Z. El; Corr, B.; Webber, G. B.; Borisenko, N.; Atkin, R.; Endres, F. In Situ STM, AFM and DTS Study of the Interface 1-Hexyl-3-Methylimidazolium Tris(pentafluoroethyl)trifluorophosphate/Au(1 1 1). *Electrochim. Acta* **2012**, *82*, 48–59.

(27) Perkin, S.; Albrecht, T.; Klein, J. Layering and Shear Properties of an Ionic Liquid, 1-Ethyl-3-Methylimidazolium Ethylsulfate, Confined to Nano-Films between Mica Surfaces. *Phys. Chem. Chem. Phys.* **2010**, *12* (6), 1243–1247.

(28) Mezger, M.; Schramm, S.; Schroder, H.; Reichert, H.; Deutsch, M.; De Souza, E. J.; Okasinski, J. S.; Ocko, B. M.; Honkimaki, V.; Dosch, H. Layering of [BMIM]+ -Based Ionic Liquids at a Charged Sapphire Interface. *J. Chem. Phys.* **2009**, *131* (9), 094701:1-9.

(29) Zhou, H.; Rouha, M.; Feng, G.; Lee, S. S.; Docherty, H.; Fenter, P.; Cummings, P. T.; Fulvio, P. F.; Dai, S.; McDonough, J.; et al. Nanoscale Perturbations of Room Temperature Ionic Liquid Structure at Charged and Uncharged Interfaces. *ACS Nano* **2012**, *6* (11), 9818–9827.

(30) Kondrat, S.; Kornyshev, A. A. Superionic State in Double-Layer Capacitors with Nanoporous Electrodes. *J. Phys. Condens. Matter* **2011**, *23* (2), 022201–022205.

(31) Vatamanu, J.; Hu, Z.; Bedrov, D.; Perez, C.; Gogotsi, Y. Increasing Energy Storage in Electrochemical Capacitors with Ionic Liquid Electrolytes and Nanostructured Carbon

Electrodes. *J. Phys. Chem. Lett.* **2013**, *4*, 2829–2837.

(32) Xing, L.; Vatamanu, J.; Borodin, O.; Bedrov, D. On the Atomistic Nature of Capacitance Enhancement Generated by Ionic Liquid Electrolyte Confined in Subnanometer Pores. *J. Phys. Chem. Lett.* **2013**, *4* (1), 132–140.

(33) Shim, Y.; Kim, H. J. Nanoporous Carbon Supercapacitors in an Ionic Liquid : A Computer Simulation. *ACS Nano* **2010**, *4* (4), 2345–2355.

(34) Kondrat, S.; Georgi, N.; Fedorov, M. V.; Kornyshev, A. A. A Superionic State in Nano-Porous Double-Layer Capacitors: Insights from Monte Carlo Simulations. *Phys. Chem. Chem. Phys.* **2011**, *13* (23), 11359–11366.

(35) Merlet, C.; Péan, C.; Rotenberg, B.; Madden, P. A.; Daffos, B.; Taberna, P.-L.; Simon, P.; Salanne, M. Highly Confined Ions Store Charge More Efficiently in Supercapacitors. *Nat. Commun.* **2013**, *4* (May), 2701:1-6.

(36) Merlet, C.; Rotenberg, B.; Madden, P. A.; Taberna, P.-L.; Simon, P.; Gogotsi, Y.; Salanne, M. On the Molecular Origin of Supercapacitance in Nanoporous Carbon Electrodes. *Nat. Mater.* **2012**, *11* (4), 306–310.

(37) Borchardt, L.; Oschatz, M.; Paasch, S.; Kaskel, S.; Brunner, E. Interaction of Electrolyte Molecules with Carbon Materials of Well-Defined Porosity: Characterization by Solid-State NMR Spectroscopy. *Phys. Chem. Chem. Phys.* **2013**, *15* (36), 15177–15184.

(38) Griffin, J. M.; Forse, A. C.; Tsai, W.-Y.; Taberna, P.-L.; Simon, P.; Grey, C. P. In Situ NMR and Electrochemical Quartz Crystal Microbalance Techniques Reveal the Structure of the Electrical Double Layer in Supercapacitors. *Nat. Mater.* **2015**, *14* (8), 812–819.

(39) Richey, F. W.; Dyatkin, B.; Gogotsi, Y.; Elabd, Y. A. Ion Dynamics in Porous Carbon Electrodes in Supercapacitors Using in Situ Infrared Spectroelectrochemistry. *J. Am. Chem. Soc.* **2013**, *135* (34), 12818–12826.

(40) Levi, M. D.; Levy, N.; Sigalov, S.; Salitra, G.; Aurbach, D.; Maier, J. Electrochemical Quartz Crystal Microbalance (EQCM) Studies of Ions and Solvents Insertion into Highly Porous Activated Carbons. *J. Am. Chem. Soc.* **2010**, *132*, 13220–13222.

(41) Levi, M. D.; Sigalov, S.; Salitra, G.; Elazari, R.; Aurbach, D. Assessing the Solvation Numbers of Electrolytic Ions Confined in Carbon Nanopores under Dynamic Charging Conditions. *J. Phys. Chem. Lett.* **2011**, *2* (2), 120–124.

(42) Levi, M. D.; Sigalov, S.; Salitra, G.; Aurbach, D.; Maier, J. The Effect of Specific Adsorption of Cations and Their Size on the Charge-Compensation Mechanism in Carbon Micropores: The Role of Anion Desorption. *ChemPhysChem* **2011**, *12* (4), 854–862.

(43) Deschamps, M.; Gilbert, E.; Azais, P.; Raymundo-Piñero, E.; Ammar, M. R.; Simon, P.; Massiot, D.; Béguin, F. Exploring Electrolyte Organization in Supercapacitor Electrodes with Solid-State NMR. *Nat. Mater.* **2013**, *12* (4), 351–358.

(44) Boukhalfa, S.; He, L.; Melnichenko, Y. B.; Yushin, G. Small-Angle Neutron Scattering for In Situ Probing of Ion Adsorption Inside Micropores. *Angew. Chemie - Int. Ed.* **2013**, *52* (17), 4618–4622.

(45) Boukhalfa, S.; Gordon, D.; He, L.; Melnichenko, Y. B.; Nitta, N.; Magasinski, A.; Yushin, G. In Situ Small Angle Neutron Scattering Revealing Ion Sorption in Microporous Capacitors. *ACS Nano* **2014**, *8* (3), 2495–2503.

(46) Wang, H.; Forse, A. C.; Griffin, J. M.; Trease, N. M.; Trognko, L.; Taberna, P.-L.; Simon, P.; Grey, C. P. In Situ NMR Spectroscopy of Supercapacitors: Insight into the Charge Storage Mechanism. *J. Am. Chem. Soc.* **2013**, *135*, 18968–18980.

(47) Griffin, J. M.; Forse, A. C.; Wang, H.; Trease, N. M.; Taberna, P.-L.; Simon, P.; Grey, C. P. Ion Counting in Supercapacitor Electrodes Using NMR Spectroscopy. *Faraday Discuss.* **2014**, *176*, 49–68.

(48) Prehal, C.; Weingarth, D.; Perre, E.; Lechner, R. T.; Amenitsch, H.; Paris, O.; Presser, V. Tracking the Structural Arrangement of Ions in Carbon Supercapacitor Nanopores Using In Situ Small-Angle X-Ray Scattering. *Energy Environ. Sci.* **2015**, *8* (6), 1725–1735.

(49) Forse, A. C.; Merlet, C.; Griffin, J. M.; Grey, C. P. New Perspectives on the Charging Mechanisms of Supercapacitors. *J. Am. Chem. Soc.* **2016**, *138*, 5731–5744.

(50) Bain, C. D. Sum-Frequency Vibrational Spectroscopy of the Solid/Liquid Interface. *J. Chem. Soc. Faraday Trans.* **1995**, *91* (9), 1281–1296.

(51) Lambert, A. G.; Davies, P. B.; Neivandt, D. J. Implementing the Theory of Sum Frequency Generation Vibrational Spectroscopy: A Tutorial Review. *Appl. Spectrosc. Rev.* **2005**, *40* (2), 103–145.

(52) Tadjeddine, A.; Peremans, A. Vibrational Spectroscopy of the Electrochemical Interface by Visible Infrared Sum-Frequency Generation. *Surf. Sci.* **1996**, *368* (1–3), 377–383.

(53) Tadjeddine, A.; Peremans, A.; Guyot-Sionnest, P. Vibrational Spectroscopy of the Electrochemical Interface by Visible-Infrared Sum-Frequency Generation. *Surf. Sci.* **1995**, *335* (C), 210–220.

(54) Lovering, K. A.; Bertram, A. K.; Chou, K. C. New Information on the Ion-Identity Dependent Structure of Stern Layer Revealed by Sum Frequency Generation Vibrational Spectroscopy. *J. Phys. Chem. C* **2016**, *120*, 18099–18104.

(55) Liu, H.; Tong, Y.; Kuwata, N.; Osawa, M.; Kawamura, J.; Ye, S. Adsorption of Propylene Carbonate (PC) on the LiCoO2 Surface Investigated by Nonlinear Vibrational Spectroscopy. *J. Phys. Chem. C* **2009**, *113* (48), 20531–20534.

(56) Yu, L.; Liu, H.; Wang, Y.; Kuwata, N.; Osawa, M.; Kawamura, J.; Ye, S. Preferential Adsorption of Solvents on the Cathode Surface of Lithium Ion Batteries. *Angew. Chemie - Int. Ed.* **2013**, *52* (22), 5753–5756.

(57) Baldelli, S. Surface Structure at the Ionic Liquid-Electrified Metal Interface. *Acc. Chem. Res.* **2008**, *41* (3), 421–431.

(58) Zhou, W.; Inoue, S.; Iwahashi, T.; Kanai, K.; Seki, K.; Miyamae, T.; Kim, D.; Katayama, Y.; Ouchi, Y. Double Layer Structure and Adsorption/Desorption Hysteresis of Neat Ionic Liquid on Pt Electrode Surface — An In-Situ IR-Visible Sum-Frequency Generation Spectroscopic Study. *Electrochem. Commun.* **2010**, *12* (5), 672–675.

(59) Zhou, W.; Xu, Y.; Ouchi, Y. Hysteresis Effects in the In-Situ SFG and Differential Capacitance Measurements on Metal Electrode/Ionic Liquids Interface. *ECS Trans.* **2012**, *50* (11), 339–348.

(60) Bozzini, B.; Bund, A.; Busson, B.; Humbert, C.; Ispas, A.; Mele, C.; Tadjeddine, A. An SFG/DFG Investigation of CN- Adsorption at an Au Electrode in 1-Butyl-1-Methyl-Pyrrolidinium Bis(trifluoromethylsulfonyl) Amide Ionic Liquid. *Electrochem. Commun.*

2010, *12* (1), 56–60.

(61) Rivera-Rubero, S.; Baldelli, S. Surface Spectroscopy of Room-Temperature Ionic Liquids on a Platinum Electrode: A Sum Frequency Generation Study. *J. Phys. Chem. B* **2004**, *108* (39), 15133–15140.

(62) Baldelli, S. Probing Electric Fields at the Ionic Liquid - Electrode Interface Using Sum Frequency Generation Spectroscopy and Electrochemistry. *J. Phys. Chem. B* **2005**, *109*, 13049–13051.

(63) Aliaga, C.; Baldelli, S. Sum Frequency Generation Spectroscopy and Double-Layer Capacitance Studies of the 1-Butyl-3-Methylimidazolium Dicyanamide-Platinum Interface. *J. Phys. Chem. B* **2006**, *110* (37), 18481–18491.

(64) Baldelli, S.; Bao, J.; Wu, W.; Pei, S. S. Sum Frequency Generation Study on the Orientation of Room-Temperature Ionic Liquid at the Graphene-Ionic Liquid Interface. *Chem. Phys. Lett.* **2011**, *516* (4–6), 171–173.

(65) Xu, S.; Xing, S.; Pei, S.-S.; Baldelli, S. Sum Frequency Generation Spectroscopy Study of an Ionic Liquid at a Graphene-BaF2 (111) Interface. *J. Phys. Chem. B* **2014**, *118* (19), 5203–5210.

(66) Xu, S.; Xing, S.; Pei, S. S.; Ivaništšev, V.; Lynden-Bell, R.; Baldelli, S. Molecular Response of 1-Butyl-3-Methylimidazolium Dicyanamide Ionic Liquid at the Graphene Electrode Interface Investigated by Sum Frequency Generation Spectroscopy and Molecular Dynamics Simulations. *J. Phys. Chem. C* **2015**, *119* (46), 26009–26019.

(67) Wang, H.; Köster, T. K.-J.; Trease, N. M.; Ségalini, J.; Taberna, P.-L.; Simon, P.; Gogotsi,

Y.; Grey, C. P. Real-Time NMR Studies of Electrochemical Double-Layer Capacitors. *J. Am. Chem. Soc.* **2011**, *133* (48), 19270–19273.

(68) Forse, A. C.; Griffin, J. M.; Merlet, C.; Bayley, P. M.; Wang, H.; Simon, P.; Grey, C. P. NMR Study of Ion Dynamics and Charge Storage in Ionic Liquid Supercapacitors. *J. Am. Chem. Soc.* **2015**, *137* (22), 7231–7242.

(69) Duffy, D. C.; Davies, P. B.; Bain, C. D. Surface Vibrational Spectroscopy of Organic Counterions Bound to a Surfactant Monolayer. *J. Phys. Chem.* **1995**, *99* (41), 15241–15246.

(70) Bell, G. R.; Bain, C. D.; Li, Z. X.; Thomas, R. K.; Duffy, D. C.; Penfold, J. Structure of a Monolayer of Hexadecyltrimethylammonium P -Tosylate at the Air - Water Interface. *J. Am. Chem. Soc.* **1997**, *119*, 10227–10228.

(71) Bell, G. R.; Li, Z. X.; Bain, C. D.; Fischer, P.; Duffy, D. C. Monolayers of Hexadecyltrimethylammonium P-Tosylate at the Air-Water Interface . 1 . Sum-Frequency Spectroscopy. *J. Phys. Chem. B* **1998**, *102*, 9461–9472.

(72) Mukherjee, P.; Lagutchev, A.; Dlott, D. D. In Situ Probing of Solid-Electrolyte Interfaces with Nonlinear Coherent Vibrational Spectroscopy. *J. Electrochem. Soc.* **2012**, *159* (3), A244–A252.

(73) Nicolau, B. G.; García-Rey, N.; Dryzhakov, B.; Dlott, D. D. Interfacial Processes of a Model Lithium Ion Battery Anode Observed, In Situ, With Vibrational Sum-Frequency Generation Spectroscopy. *J. Phys. Chem. C* **2015**, *119* (19), 10227–10233.

(74) Horowitz, Y.; Han, H. L.; Ross, P. N.; Somorjai, G. A. In Situ Potentiodynamic Analysis

of the Electrolyte/Silicon Electrodes Interface Reactions - A Sum Frequency Generation Vibrational Spectroscopy Study. *J. Am. Chem. Soc.* **2016**, *138* (3), 726–729.

(75) Battisti, D.; Nazri, G. A.; Klassen, B.; Aroca, R. Vibrational Studies of Lithium Perchlorate in Propylene Carbonate Solutions. *J. Phys. Chem.* **1993**, *97* (22), 5826–5830.

(76) Wang, J.; Wu, Y.; Xuan, X.; Wang, H. Ion-Molecule Interactions in Solutions of Lithium Perchlorate in Propylene Carbonate + Diethyl Carbonate Mixtures: An IR and Molecular Orbital Study. *Spectrochim. Acta - Part A Mol. Biomol. Spectrosc.* **2002**, *58* (10), 2097–2104.

(77) Arjunan, V.; Saravanan, I.; Ravindran, P.; Mohan, S. FTIR, FT-Raman, Ab Initio and Density Functional Studies on 4-Methyl-1,3-Dioxolan-2-One and 4,5-Dichloro-1,3-Dioxolan-2-One. *Spectrochim. Acta Part A Mol. Biomol. Spectrosc.* **2010**, *77* (1), 28–35.

(78) Gorobets, M. I.; Ataev, M. B.; Gafurov, M. M.; Kirillov, S. A. Raman Study of Solvation in Solutions of Lithium Salts in Dimethyl Sulfoxide, Propylene Carbonate and Dimethyl Carbonate. *J. Mol. Liq.* **2015**, *205*, 98–109.

(79) Casford, M. T. L.; Davies, P. B.; Neivandt, D. J. Study of the Coadsorption of an Anionic Surfactant and an Uncharged Polymer at the Aqueous Solution/Hydrophobic Surface Interface by Sum Frequency Spectroscopy. *Langmuir* **2003**, *19* (18), 7386–7391.

(80) Casford, M. T. L.; Davies, P. B. The Structure of Oleamide Films at the Aluminum/Oil Interface and Aluminum/Air Interface Studied by Sum Frequency Generation (SFG) Vibrational Spectroscopy and Reflection Absorption Infrared Spectroscopy (RAIRS). *ACS Appl. Mater. Interfaces* **2009**, *1* (8), 1672–1681.

(81) Wood, M. H.; Casford, M. T.; Steitz, R.; Zarbakhsh, A.; Welbourn, R. J. L.; Clarke, S. M. Comparative Adsorption of Saturated and Unsaturated Fatty Acids at the Iron Oxide/Oil Interface. *Langmuir* **2016**, *32* (2), 534–540.

(82) Lu, R.; Gan, W.; Wu, B.; Zhang, Z.; Guo, Y.; Wang, H. C-H Stretching Vibrations of Methyl , Methylene and Methine Groups at the Vapor/Alcohol (n=1-8) Interfaces. *J. Phys. Chem. B* **2005**, *109*, 14118–14129.

(83) Lu, R.; Gan, W.; Wu, B.; Chen, H.; Wang, H. Vibrational Polarization Spectroscopy of CH Stretching Modes of the Methylene Group at the Vapor/Liquid Interfaces with Sum Frequency Generation. *J. Phys. Chem. B* **2004**, *108*, 7297–7306.

(84) Ristova, M.; Pejov, L.; Žugić, M.; Šoptrajanov, B. Experimental IR, Raman and Ab Initio Molecular Orbital Study of the 4-Methylbenzenesulfonate Anion. *J. Mol. Struct.* **1999**, *482–483*, 647–651.

(85) Pejov, L.; Ristova, M.; Soptrajanov, B. Quantum Chemical Study of P-Toluenesulfonic Acid, P-Toluenesulfonate Anion and the Water-P-Toluenesulfonic Acid Complex. Comparison with Experimental Spectroscopic Data. *Spectrochim. Acta Part A Mol. Biomol. Spectrosc.* **2011**, *79* (1), 27–34.

(86) Aliaga, C.; Baker, G. A.; Baldelli, S. Sum Frequency Generation Studies of Ammonium and Pyrrolidinium Ionic Liquids Based on the Bis-Trifluoromethanesulfonimide Anion. *J. Phys. Chem. B* **2008**, *112* (6), 1676–1684.

(87) Konarev, D. V.; Kuzmin, A. V.; Khasanov, S. S.; Otsuka, A.; Yamochi, H.; Saito, G.; Lyubovskaya, R. N. Design, Crystal Structures and Magnetic Properties of Anionic Salts

Containing Fullerene C60 and Indium(III) Bromide Phthalocyanine Radical Anions. *Dalt. Trans.* **2014**, *43*, 13061–13069.

(88) Konarev, D. V.; Kuzmin, A. V.; Faraonov, M. A.; Ishikawa, M.; Khasanov, S. S.; Nakano, Y.; Otsuka, A.; Yamochi, H.; Saito, G.; Lyubovskaya, R. N. Synthesis, Structures, and Properties of Crystalline Salts with Radical Anions of Metal-Containing and Metal-Free Phthalocyanines. *Chem. A Eur. J.* **2015**, *21* (3), 1014–1028.

(89) Scheu, R.; Chen, Y.; Subinya, M.; Roke, S. Stern Layer Formation Induced by Hydrophobic Interactions: A Molecular Level Study. *J. Am. Chem. Soc.* **2013**, *135*, 19330–19335.

(90) Tsai, W.-Y.; Taberna, P.-L.; Simon, P. Electrochemical Quartz Crystal Microbalance (EQCM) Study of Ion Dynamics in Nanoporous Carbons. *J. Am. Chem. Soc.* **2014**, *136* (24), 8722–8728.

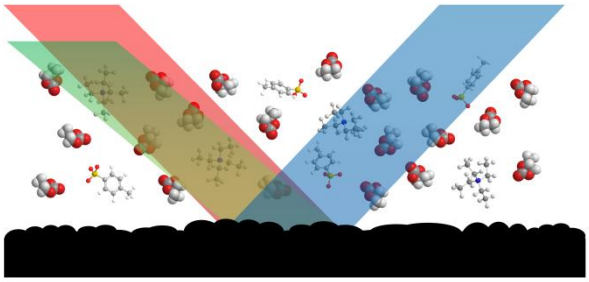

TOC graphic